Current Enzyme Inhibition, 2017, *13*, 184-190

RESEARCH ARTICLE

Characterization of a New Allelic Variant of Triosephosphate Isomerase from the LNCaP Human Prostate Cancer Cell Line: Enzyme Inhibition and Spectroscopic Studies

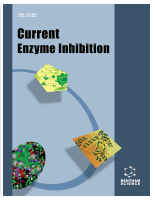

Valeria Guzmán-Luna, Leticia Olvera-Rodríguez, Peniel Bustamante-Villalobos and Gloria Saab-Rincón*

Departamento de Ingeniería Celular y Biocatálisis, Instituto de Biotecnología, Universidad Nacional Autónoma de México, Apdo. Postal 510-3, 62250 Cuernavaca, Morelos, México

ARTICLE HISTORY

Received: August 06, 2016
Revised: August 29, 2016
Accepted: September 05, 2016

DOI:
10.2174/1573408012666160906110330

Abstract: ***Background*:** The glycolytic pathway plays an important role in tumor cells. Triosephosphate isomerase (TIM) catalyzes the reversible isomerization of D-glyceraldehyde-3-phosphate (GAP) to dihydroxyacetone phosphate (DHAP) in the glycolysis. Proteomics of a human prostate adenocarcinoma cell line revealed the presence of the G233D TIM variant, a new allelic type whose biochemical properties have not been reported [1].

***Objective*:** Provide the first biochemical and biophysical characterization of the allelic variant G233D of TIM.

***Methods*:** The Michaelis-Menten curves using both substrates of TIM were obtained. Also the effect of the competitive inhibitor phosphoenolpyruvate (PEP) was assessed in presence of GAP and DHAP. The thermal stability in absence and presence of PEP was analyzed by circular dichroism spectroscopy. For comparison purposes, all the measurements were carried out on the wild type TIM and variant G233D.

***Results*:** The G233D variant exhibited a k_{cat} value 4-fold lower than that of the WT enzyme in the GAP isomerization to DHAP, which is the reverse reaction of the glycolytic pathway. The G233D variant exhibited Ki and IC_{50} values of 120 μM and 356 μM in the presence of several concentrations of GAP and 0.3 mM DHAP, respectively. These inhibition parameters are similar to those exhibited by the WT enzyme. The thermal unfolding cooperativity of G233D variant was significantly increased upon PEP binding, suggesting that the ligand-bound enzyme was trapped in a rigid conformation.

***Conclusion*:** We suggest that the flow of GAP through glycolysis could be enhanced by the decreased activity of the G233D variant in the formation of DHAP.

Keywords: Allelic variant, glyceraldehyde-3-phosphate, glycolysis, human prostate cancer, phosphoenolpyruvate, triosephosphate isomerase.

1. INTRODUCTION

Altered glucose metabolism is one of the hallmarks of cancer. Despite the presence of oxygen, cancer cells reprogram their energy metabolism largely to anaerobic glycolysis and lactate secretion [2-5]. Triosephosphate isomerase (TIM) plays an essential role in glycolysis, gluconeogenesis, fatty acid synthesis, and in the pentose phosphate pathway (PPP) [6]. TIM is a homodimeric enzyme that interconverts dihydroxyacetone phosphate (DHAP) and glyceraldehyde-3-phosphate (GAP), causing a rapid equilibrium of triosephosphates in favor of DHAP formation by 22-fold at 38°C and pH 7.5 (96% DHAP and 4% GAP) [7]. Because only GAP completes glycolysis, TIM prevents the accumulation of DHAP [8], which could deplete intracellular ATP, the trapping of inorganic phosphate, and/or the formation of toxic methylglyoxal [9]. Interestingly, TIM has been found in increased concentrations in lung cancers [10], squamous cell lung carcinomas [11], urinary cancers [12], and chemoresistant ovarian carcinoma cell lines [13]. This suggests its direct participation in the increased anaerobic glycolysis observed in cancer cells [14]. A proteomic study of the LNCaP human prostate adenocarcinoma cell line found a new allelic variant of human TIM (HsTIM), the G233D variant [1]. Gly-233 is located at the N-terminus of loop-8 (PDBID 1HTI) of the $(\beta/\alpha)_8$ TIM barrel and is considered a substrate-binding residue [15]. The active site geometry of the structure of the

*Address correspondence to this author at the Departamento de Ingeniería Celular y Biocatálisis, Instituto de Biotecnología, Universidad Nacional Autónoma de México, Apdo. Postal 510-3, 62250 Cuernavaca, Mor., México; Tel: +52 (777) 329-1640; E-mail: gsaab@ibt.unam.mx

1875-6662/17 $58.00+.00

TIM-PGH complex at 0.82 Å resolution (PDBID 2VXN) shows a phosphate-dianion binding pocket. The latter is composed of four main chain NH-groups from loop-6 (Gly-172), loop-7 (Ser-213) and loop-8 (Gly-233 and Gly-234) that bind to the phosphate-dianion moiety of the ligand *via* hydrogen bonds [8]. In the present study, we report for the first time the kinetic, spectroscopic and thermal stability properties of the recombinant G233D mutant of HsTIM. Additionally, we analyzed the susceptibilities of the WT HsTIM and G233D mutant to the weak inhibitor phosphoenolpyruvate (PEP) [16]. The crucial metabolic role of PEP to simultaneously modulate the flow of glycolysis and the PPP has been demonstrated by *in vivo* studies, which showed that increased PEP concentrations stimulated the PPP pathway due to the inhibition of TIM activity [17]. Because the PPP provides nucleotides, this pathway is positively regulated in rapidly growing cells, including cells of multiple cancer types [18].

Overall, this work had two aims: 1) provide the first kinetic and biophysical characterization of the cancer-related G233D variant of HsTIM, and 2) provide a structural rationalization of the interactions in which the Asp-233 side chain could participate using molecular modeling of the *in silico* mutant.

2. MATERIALS AND METHODS

2.1. Site-directed Mutagenesis

The G233D mutation was achieved using site-directed mutagenesis using PCR and the appropriate mutagenic oligonucleotides. The PCR products were cloned into the pET28b vector after digestion with NdeI and BamHI restriction enzymes. After confirming the presence of the desired mutation by DNA sequencing, we used the mutant plasmid to transform a *tpi*- strain of *E.coli* BL21(DE3) cells (Novagen).

2.2. Protein Expression and Purification

Transformed cells were grown in LB medium supplemented with ampicillin at 30°C until an absorbance of 0.6 at 600 nm was reached. Then, the expression of TIM was induced with 0.2 mM IPTG (final concentration). Incubation continued at 18°C for 16 h. The cells were harvested and suspended in buffer A (20 mM sodium phosphate, 150 mM NaCl, pH 8.0). The cell suspension was sonicated and centrifuged at 12,000 g for 30 min. The supernatant was loaded onto a Ni-NTA agarose column, and the TIM protein was then eluted using a gradient from 5 to 500 mM imidazole in buffer A. The purified HsTIM was dialyzed against four changes of buffer A to eliminate the imidazole. The sequence of the wild-type HsTIM gene encodes a His-6X tag at the N-terminus followed by a TEV protease recognition sequence. The His-6X tag was cleaved using recombinant His-tagged TEV protease at a ratio of 1:25 (w/w) protease:HsTIM at 4°C overnight. The mixture was loaded onto a Ni-NTA agarose column and washed with buffer A to separate the His-tagged TEV protease and any undigested HsTIM. The effluent from the column containing the cleaved HsTIM was recovered, and its purity was assessed using SDS-PAGE. The protein concentration was determined by measuring the absorbance at 280 nm using a theoretical extinction coefficient of ε= 33,460 $M^{-1}cm^{-1}$ obtained from the ProtParam tools of the Expasy Proteomics Server [19].

2.3. Enzyme Kinetics Assays

All reagents were purchased from Sigma-Aldrich (St. Louis, MO, USA). The enzymatic activity was measured using coupled assays that monitored the absorbance signal at 340 nm. To study the forward reaction (formation of GAP), a 50 mM Tris-HCl (pH 7.5), 0.5 mM EDTA buffer was used containing 0.2 mM NADH, 20 μg/mL glycerol-3-phosphate dehydrogenase as the coupling enzyme and GAP concentrations from 0.1 to 1.0 mM. The solutions were equilibrated at 25 °C and the reaction was initiated by the addition of 10 ng of TIM in a final volume of 1 mL. To study the reverse reaction (formation of DHAP), a 50 mM Tris-HCl (pH 7.5), 0.5 mM EDTA buffer containing 1 mM NAD^+, 2 units of glyceraldehyde-3-phosphate dehydrogenase as the coupling enzyme, 4 mM sodium arsenate, 0.12 mM DTT, DHAP concentrations from 0.05 to 0.5 mM were used and equilibrated at 25 °C. The reaction was initiated by adding 200 ng of TIM in a final volume of 0.7 mL. The initial rates were calculated from the change in absorbance at 340 nm with a Beckman DU-730 spectrophotometer at 25°C. To study the inhibition of TIM, the TIM's substrate analog phosphoenolpyruvate (PEP, from Sigma), was added to the final concentrations indicated in Fig. (**2**). The inhibition assays were carried out as described above. The data were adjusted to the Michaelis-Menten model, and the Km and Vmax values were calculated using a non-linear regression model with the OriginPro software (version 8.0). To obtain the Ki, the GAP-saturation curve in presence of different concentrations of the reversible-competitive inhibitor PEP were fitted to a Michaelis-Menten equation, as indicated in Equation 1:

$$vo = \frac{\text{Vmax}\,[\text{GAP}]}{\text{Km}_{\text{app}} + [\text{GAP}]} \quad (1)$$

Afterwards, the obtained Km_{app} values were plotted against the PEP concentrations to obtain the value of Ki from the slope of the following linear relationship:

$$\text{Km}_{\text{app}} = \text{Km} + [\text{PEP}]\frac{\text{Km}}{\text{Ki}} \quad (2)$$

where Km is the value in absence of inhibitor.

2.4. Circular Dichroism and Thermal Stability

Circular dichroism (CD) spectra were recorded using a Jasco J-715 CD spectropolarimeter (JASCO Analytical Instruments) equipped with a Peltier temperature-controlled cell holder (PTC-4235, JASCO). The far-UV spectra (190-260 nm) were recorded using a 0.1 cm path length quartz cell. Three spectra were averaged to reduce noise. Spectra were acquired every 1 nm, with eight seconds average time per point and 1 nm band pass. The temperature dependence of the secondary structure was studied by monitoring the CD signal at 220 nm. Experiments were performed with at least three independent, freshly prepared samples in 10 mM nylon-filtered (0.22 μm) phosphate buffer (pH 7.4) and 200 μg/mL of protein. The temperature range monitored was 15-80°C. PEP was added to a final concentration of 2.5 mM, and then the thermal stability was reassessed.

Table 1. Kinetic parameters of WT HsTIM and the G233D mutant at 25°C.

Parameter	Substrate	Variant	
		WT	G233D
Km (mM)	GAP	0.14±0.01	0.18±0.05
	DHAP	0.18±0.03	0.13±0.02
Vmax (μmol/(min-mg))	GAP	8965±218	2425±264
	DHAP	5.9±0.4	5.1±0.2
k_{cat} (min^{-1})	GAP	$2.4x10^5$±$6x10^4$	$6.4x10^4$±$7x10^3$
	DHAP	$1.5x10^2$±10	$1.4x10^2$±6
k_{cat}/Km ($min^{-1}M^{-1}$)	GAP	$1.7x10^9$	$3.6x10^8$
	DHAP	$8.3x10^5$	$1.1x10^6$
Ki[a] (μM)	GAP	123±5.0	120±5.2
IC_{50}[b] (μM)	DHAP	357±70	356±37

[a]Inhibition constants were obtained with GAP concentrations ranging from 0.1 to 0.45 mM. [b]Obtained at a concentration of 0.3 mM DHAP and PEP concentrations ranging from 1 to 5 mM.

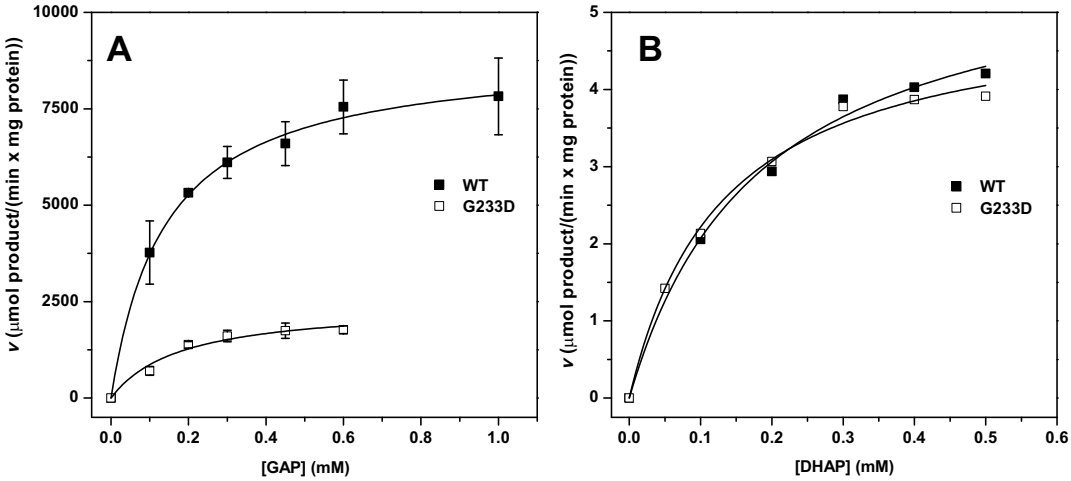

Fig. (1). Kinetic analysis of WT HsTIM (black squares) and the G233D variant (open squares) at 25°C. Panel A. DHAP formation. The incubation mixture contained GAP concentrations from 0.1 to 1.0 mM and 10 ng of TIM in a final volume of 1 mL. Panel B. GAP formation. The incubation mixture contained DHAP concentrations from 0.05 to 0.5 mM and 200 ng of TIM in a final volume of 0.7 mL. The reported values are averages of at least three independent determinations. Solid lines are fit to the Michaelis-Menten equation.

2.5. Molecular Modelling

The *in silico* G233D mutant model was constructed with PyMOL using the structure of the closed and open monomers of WT HsTIM (PDB ID: 1HT1) as a template (http://sourceforge.pymol.org). To optimize geometries, release local constraints, and correct possible inappropriate contacts, the energy minimization of the structures was carried out using the ModRefiner algorithm [20].

3. RESULTS

3.1. Enzyme Kinetics and Inhibition

Catalytic activity measurements were carried out in both senses of the isomerization reaction. The Michaelis-Menten saturation curves, in which initial velocity is plotted as a function of substrate, are shown in Fig. (**1**) for both GAP and DHAP. The kinetic parameters Km, Vmax, and k_{cat} were determined using non-linear fits to the Michaelis-Menten equation, and the resulting parameters are listed in Table **1**. When DHAP was used as the substrate, the WT enzyme and the G233D mutant exhibited the same k_{cat} and Km. In contrast, with GAP as the substrate, the value of k_{cat} for the G233D mutant was decreased by almost 4-fold compared to that of the WT enzyme (Table **1**). The isomerization of GAP to DHAP catalyzed by TIM is diffusion-controlled. Accordingly, the ratios of k_{cat}/Km for the WT TIM and G233D mutant were on the order of 10^8 to 10^9 $M^{-1}s^{-1}$, as expected for the diffusion limit [21]. We carried out inhibition experiments to determine the effect of the physiologically relevant PEP metabolite on the catalytic activity of the HsTIM variant. To calculate the value of the inhibition constants, the GAP saturation curves in the presence of different PEP con-

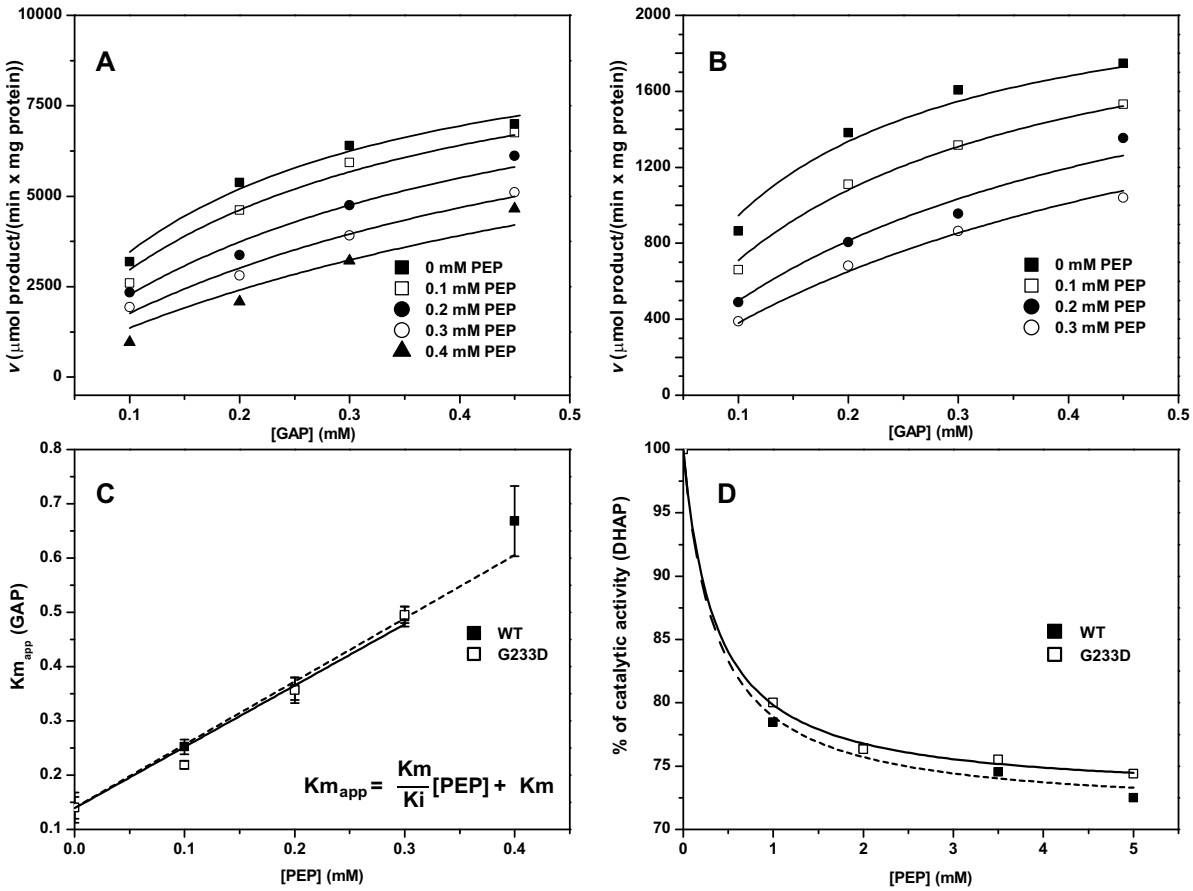

Fig. (2). Panels A and B. The catalytic activities of WT TIM (Panel A) and the G233D variant (Panel B) were measured at a range of GAP concentrations in the presence of increasing PEP concentrations. Apparent Km values (Km_{app}) were determined by fitting the data to the Michaelis-Menten equation using OriginPro (version 8.0) software. Panel C. Apparent Km values at increasing PEP concentrations. The linear dependence of Km_{app} on PEP concentrations indicates a competitive mechanism of inhibition. Panel D. Residual activity of TIM variants at 0.3 mM of DHAP in the presence of increasing PEP concentrations. The solid line is the fit to a hyperbola decreasing function.

centrations were obtained, and data were fit to the Michaelis-Menten equation (Fig. **2A** and **2B**). PEP has been previously demonstrated to be a weak competitive inhibitor of TIM [16, 17, 22]; therefore, the values of Km should increase in the presence of PEP. Accordingly, the apparent Km (Km_{app}) values increased linearly with PEP concentrations in the range of 0.1 to 0.4 mM (Fig. **2C**). Values of Ki were calculated from the linear fits of the data shown in Fig. (**2C**) using the slope (Km/Ki) and the y-intercept (Km) of the equation shown in the inset. Table **1** shows that in the presence of GAP, the WT and G233D variants have the same Ki values, which are on the micromolar order. These Ki values are close to those reported for rabbit and human TIMs, which are 500 μM and 163 μM, respectively [16, 17]. Additionally, at a concentration of 0.3 mM DHAP, the IC_{50} of PEP inhibition was approximately 350 μM for both TIM variants (Fig. **2D** and Table **1**).

3.2. Thermal Stability

The temperature-induced unfolding transitions were studied by following the circular dichroism (CD) signal at 220 nm. Samples were heated in the absence and presence of 2.5 mM PEP at a rate of 1°C/min (Fig. **3A** and **3B**). In both conditions variants underwent a single transition to an unfolded state that contained significantly less helical content compared to the native conformations. To analyze the conformational transitions, data were fit to a Boltzmann sigmoidal equation. We calculated the midpoint of the unfolding transition (Tm_{app}) and the apparent cooperativity coefficient (n). The resulting values are plotted in Fig. (**3C**). The Tm_{app} indicated that the G233D mutation decreases the midpoint of the transition by 1.5°C compared to the WT enzyme. While the presence of PEP did not increase the Tm_{app} in the WT variant, the PEP-bound G233D variant exhibited a Tm_{app} value similar to that of the ligand-free WT variant. Fig. (**3C**) shows that upon PEP-binding, the WT and G233D mutant variants exhibited higher cooperativity indexes compared with the transitions of the ligand-free protein conformations. Note that the value of the *n* coefficient is directly proportional to the cooperativity of the protein thermal unfolding. This can be explained by the formation of interactions upon PEP-binding, such as the closure of loop-6 over the TIM active-site and the hydrogen bonds formed with the phosphate moiety of the ligand [8]. Because both PEP-bound variants exhibited very similar Tm_{app} and *n* index values (Fig. **3C**), we propose that upon PEP-binding the conformation of the G233D mutant changes to a structure closely resembling that of the PEP-bound WT enzyme. Far-UV CD measurements were carried out to determine the enzyme conformational

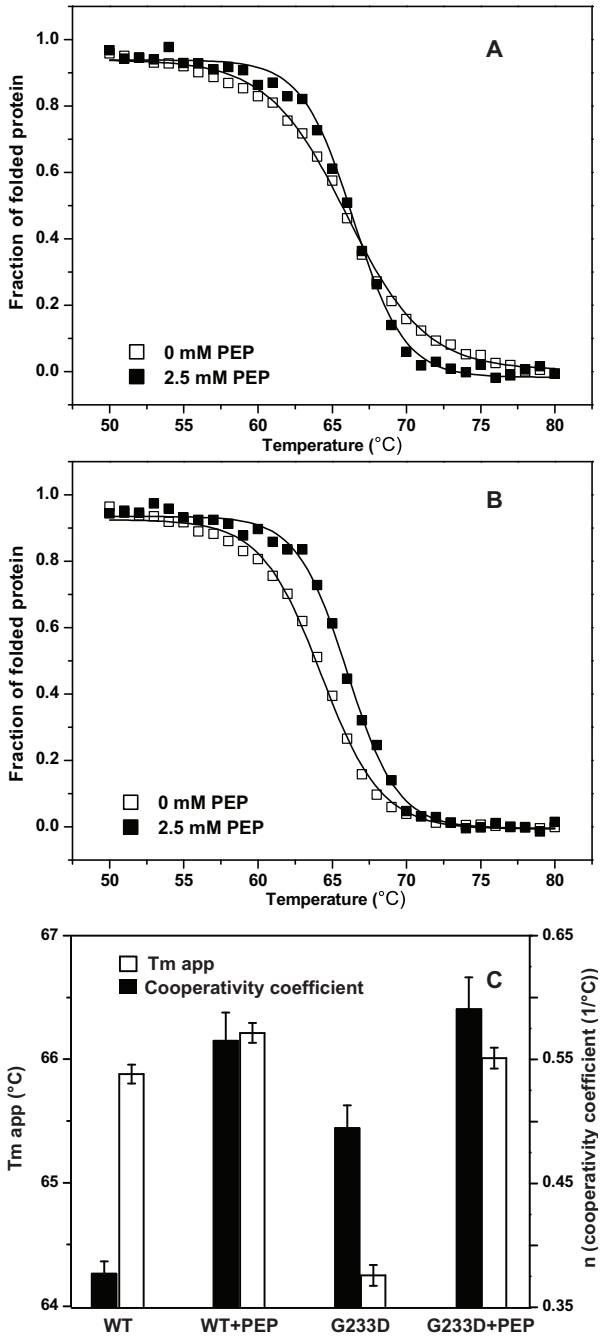

Fig. (3). Temperature-induced conformational transitions of WT HsTIM (Panel A) and the G233D mutant (Panel B) in the absence or presence of PEP (open and black squares, respectively) monitored using CD at 220 nm. Continuous lines were fit to single-sigmoid functions. Experiments were performed at protein concentrations of 0.2 mg/mL. Data represent the average of three independent experiments, as explained in the Materials and Methods section. Error bars were removed for clarity. Panel C. Tm_{app} and unfolding cooperativity index values.

changes occurring after PEP binding. While all of the collected spectra were consistent with spectra for β/α barrels, the spectra of the PEP-bound forms exhibited a higher content of α-helices, as indicated by the increased CD signal at 208 nm (Fig. **4A** and **4B**). Importantly, comparison between the CD spectra of the free G233D mutant and the WT enzyme indicates that the G233D mutation increases the CD signal by 20% at 220 nm, which corresponds to α-helical structure. Finally, the PEP-free G233D mutant exhibited a significantly more cooperative unfolding transition compared to the PEP-free WT enzyme. This could be explained by a more rigid conformation of the mutant due to the presence of polar interactions mediated by the Asp-233 side chain. We carried out a molecular modeling analysis to rationalize such behavior.

3.3. Molecular Modeling

The differences between the contact maps of the minimized structures of the WT enzyme and the G233D mutant (cutoff 4 Å) indicated that the side chain of Asp-233 is in contact with residues of the active site. Fig. (**5A**) shows the position of important amino acids of the active site of HsTIM in the closed conformation. His-95 and Glu-165 participate in the catalytic mechanism of TIM [8], and Lys-13 stabilizes the negatively charged phosphate of substrates. Fig. (**5A**) also shows the Asp-233 side chain of the *in silico* mutant. The G233D mutation decreased k_{cat} 4-fold in the reverse direction (GAP to DHAP), whereas in the forward direction (DHAP to GAP), both variants showed the same kinetic parameters. Thus, the presence of the Asp-233 side chain changed the rate of a limiting step(s) of the reverse reaction. In the WT TIM, this is a proton transfer step related to product formation [23, 24]. In the open conformation of the active site, the side chain of Asp-233 participates in a hydrogen bond network absent in the WT structure that connects Lys-13 with Asn-11, Gly-234, and Ser-236 residues (Fig. **5B**). The same as Lys-13, Asn-11 is important for substrate electrostatic stabilization [25-27]. Therefore, the increased cooperativity index of thermal unfolding of the G233D mutant may suggest a more rigid structure mediated by either of the interactions shown in Fig. (**5**).

DISCUSSION & CONCLUSION

We studied the biochemical and biophysical properties of the G233D mutant, an uncharacterized variant of triosephosphate isomerase found in a prostate cancer cell line [1]. The G233D variant and the WT enzyme exhibited the same binding affinity for the GAP, DHAP and PEP. These results were unexpected because according to the modeled structure of G233D mutant, the side chain of Asp-233 points inward to the active site (Fig. **5B**). Structural modeling of the G233D mutant was carried out using both the free and the ligand-bound structures. However, in the latter, the side chain of Asp-233 clashed with the negatively charged phosphate of the ligand (data not shown). Because the main chain NH-groups from residues 233 and 234 bind to the phosphate-dianion moiety of the ligand [8], it can be speculated that the side chain of Asp-233 faces outwards of the active site in the ligand-bound structure. This could be facilitated by the presence of the adjacent residue Gly-234, thus avoiding steric hindrance with the side chain of Asp-233. The presence of major structural changes of the ligand binding residues and/or catalytic residues upon G233D mutation can be dismissed, since the G233D variant and the WT enzyme exhibited the same catalytic parameters in the formation of GAP.

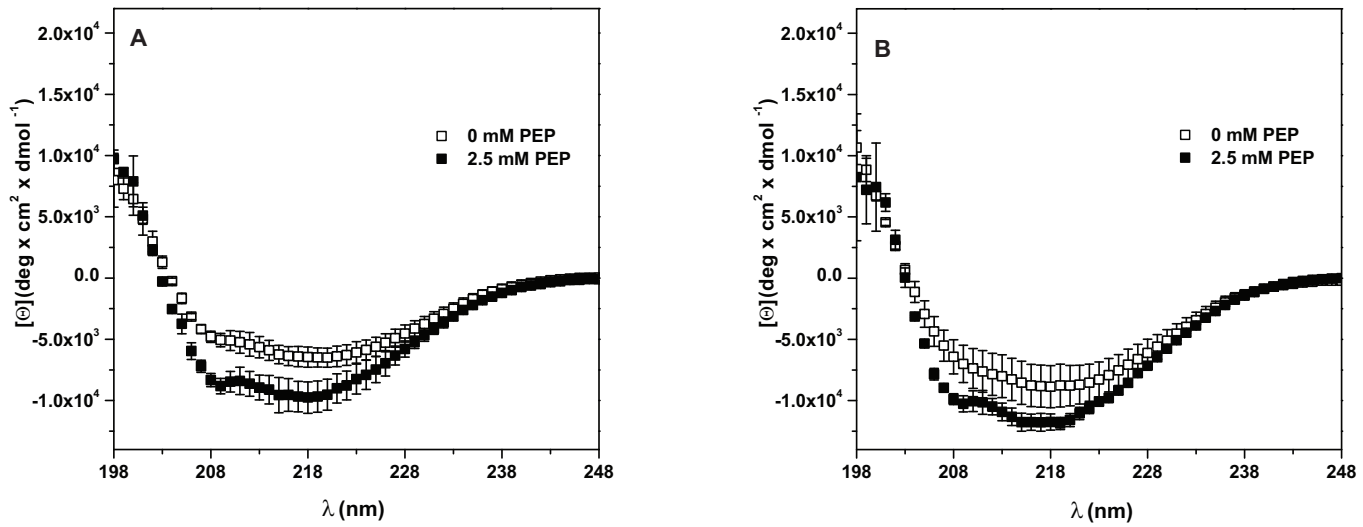

Fig. (4). Far-UV CD spectra of WT HsTIM (Panel A) and the G233D variant (Panel B) in the presence and absence of PEP. All spectra were recorded at 25°C at a TIM concentration of 0.2 mg/mL.

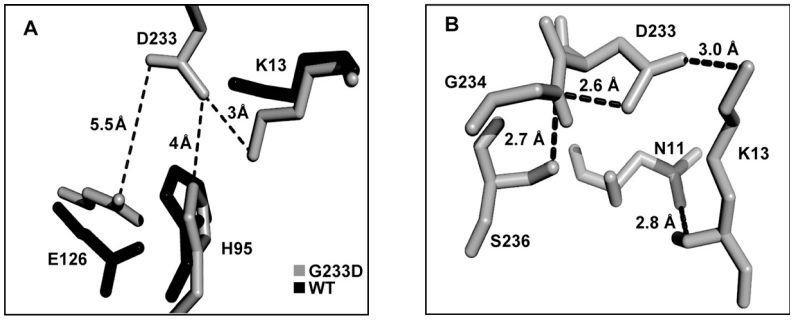

Fig. (5). The position of amino acids interacting less than 4 Å from the D233 side-chain as modeled in the *in silico* mutant. Panel A. Hydrogen bond network in the open conformation of the active site (PDBID 1HTI, chain **A**). Panel B. Comparison of catalytic residues of the closed conformation of the active site in the structures of WT HsTIM and the G233D mutant (PDBID 1HTI, chain **B**).

On the other hand, the G233D variant exhibited a k_{cat} value almost 4-fold lower than that of the WT in the reverse reaction of the glycolytic pathway (GAP to DHAP). These results suggest that the homodimeric G233D mutant could increase the flow of GAP through glycolysis under cellular conditions. Importantly, GAP is also a substrate of glyceraldehyde-3-phosphate dehydrogenase (GAPDH), which has a key role in the metabolism of tumor cells. In particular, overexpression of GAPDH has been considered an important feature of many types of cancer cells [14, 28]. However, it is necessary to consider the cellular metabolic environment and the intracellular concentrations of the metabolites that can influence TIM activity in prostate cancer cells. Finally, while this study provides the first kinetic and biophysical characterization of the new allelic G233D HsTIM mutant, several questions remain to be answered, for instance, the possibility of heterodimer formation between WT and G233D monomers, direct measurement of TIM activity in prostate cancer cells and the elucidation of the three-dimensional crystal structure of the G233D mutant.

CONFLICT OF INTEREST

The authors declare no conflict of interest, financial or otherwise.

ACKNOWLEDGEMENTS

The pET3a-HsTIM vector was kindly donated by Professor Gomez Puyou (IFC-UNAM). We thank Biol. Filiberto Sánchez-López and Dr. Edson Cárcamo-Noriega for assistance in the purification of WT HsTIM. We also thank Plácido Daniel Hernández Sánchez and Janeth Ramón Guerrero for their assistance with mutagenesis experiments. VGL is the grateful recipient of a DGAPA-UNAM postdoctoral scholarship. This work was supported the Programa de Apoyo a Proyectos de Investigación e Innovación Tecnológica (PAPIIT) (grant number IN211414 to GSR).

REFERENCES

[1] Kovalev, L.I.; Makarov, A.A.; Cherkashin, E.A.; Dulinska, J.; Kovaleva, M.A.; Lisitskaya, K.V.; Ivanov, A.V.; Toropygin, I.Y.; Serebryakova, M.V.; Laidler, P.; Shishkin, S.S. New allelic variant of triosephosphate isomerase found in cultured tumor cells of human prostate. *Mol. Genet. Microbiol. Virol.,* **2011**, *26*, 14-20.

[2] Warburg, O. On the origin of cancer cells. *Science,* **1956**, *123*, 309-14.

[3] Hsu, P.P.; Sabatini, D.M. Cancer cell metabolism: Warburg and beyond. *Cell,* **2008**, *134*, 703-707.

[4] Najafov, A.; Alessi, D.R. Uncoupling the Warburg effect from cancer. *Proc. Natl. Acad. Sci. U.S.A.,* **2010**, *107*, 19135-19136.

[5] Levine, A.J.; Puzio-Kuter, A.M. The control of the metabolic switch in cancers by oncogenes and tumor suppressor genes. *Science,* **2010**, *330*, 1340-1344.

[6] Orosz, F.; Olah, J.; Ovadi, J. Triosephosphate isomerase deficiency: facts and doubts. *IUBMB life,* **2006**, *58*, 703-715.

[7] Veech, R.L.; Raijman, L.; Dalziel, K.; Krebs, H.A. Disequilibrium in the triose phosphate isomerase system in rat liver. *Biochem. J.,* **1969**, *115*, 837-42.

[8] Wierenga, R.K.; Kapetaniou, E.G.; Venkatesan, R. Triosephosphate isomerase: A highly evolved biocatalyst. *Cellular and molecular life sciences: CMLS,* **2010**, *67*, 3961-3982.

[9] Ciriacy, M.; Breitenbach, I. Physiological effects of seven different blocks in glycolysis in *Saccharomyces cerevisiae*. *J. Bacteriol.,* **1979**, *139*, 152-60.

[10] Chen, G.; Gharib, T.G.; Huang, C.C.; Thomas, D.G.; Shedden, K.A.; Taylor, J.M.; Kardia, S.L.; Misek, D.E.; Giordano, T.J.; Iannettoni, M.D.; Orringer, M.B.; Hanash, S.M.; Beer, D.G. Proteomic analysis of lung adenocarcinoma: Identification of a highly expressed set of proteins in tumors. *Clin. Cancer Res.,* **2002**, *8*, 2298-2305.

[11] Li, C.; Xiao, Z.; Chen, Z.; Zhang, X.; Li, J.; Wu, X.; Li, X.; Yi, H.; Li, M.; Zhu, G.; Liang, S. Proteome analysis of human lung squamous carcinoma. *Proteomics,* **2006**, *6*, 547-558.

[12] Unwin, R.D.; Craven, R.A.; Harnden, P.; Hanrahan, S.; Totty, N.; Knowles, M.; Eardley, I.; Selby, P.J.; Banks, R.E. Proteomic changes in renal cancer and co-ordinate demonstration of both the glycolytic and mitochondrial aspects of the Warburg effect. *Proteomics,* **2003**, *3*, 1620-1632.

[13] Di Michele, M.; Marcone, S.; Cicchillitti, L.; Della Corte, A.; Ferlini, C.; Scambia, G.; Donati, M.B.; Rotilio, D. Glycoproteomics of paclitaxel resistance in human epithelial ovarian cancer cell lines: Towards the identification of putative biomarkers. *J. Proteomics,* **2010**, *73*, 879-898.

[14] Lincet, H.; Icard, P. How do glycolytic enzymes favour cancer cell proliferation by nonmetabolic functions? *Oncogene,* **2015**, *34*, 3751-3759.

[15] Schneider, A.S. Triosephosphate isomerase deficiency: Historical perspectives and molecular aspects. Bailliere's best practice & research. *Clinical Haematol,* **2000**, *13*, 119-140.

[16] Lambeir, A.M.; Opperdoes, F.R.; Wierenga, R.K. Kinetic properties of triose-phosphate isomerase from *Trypanosoma brucei brucei*. A comparison with the rabbit muscle and yeast enzymes. *European J. Biochem.*, *FEBS,* **1987**, *168*, 69-74.

[17] Gruning, N.M.; Rinnerthaler, M.; Bluemlein, K.; Mulleder, M.; Wamelink, M.M.; Lehrach, H.; Jakobs, C.; Breitenbach, M.; Ralser, M. Pyruvate kinase triggers a metabolic feedback loop that controls redox metabolism in respiring cells. *Cell Metab.,* **2011**, *14*, 415-427.

[18] Tsouko, E.; Khan, A.S.; White, M.A.; Han, J.J.; Shi, Y.; Merchant, F.A.; Sharpe, M.A.; Xin, L.; Frigo, D.E. Regulation of the pentose phosphate pathway by an androgen receptor-mTOR-mediated mechanism and its role in prostate cancer cell growth. *Oncogenesis,* **2014**, *3*, e103.

[19] Gasteiger, E.; Hoogland, C.; Gattiker, A.; Duvaud, S.E.; Wilkins, M.R.; Appel, R.D.; Bairoch, A. Protein identification and analysis tools on the ExPASy server. In: *The Proteomics Protocols Handbook*, In: Walker, J.M., Eds. Humana Press: Totowa, NJ, **2005**; pp. 571-607.

[20] Xu, D.; Zhang, Y. Improving the physical realism and structural accuracy of protein models by a two-step atomic-level energy minimization. *Biophys. J.,* **2011**, *101*, 2525-2534.

[21] Albery, W.J.; Knowles, J.R. Evolution of enzyme function and the development of catalytic efficiency. *Biochemistry,* **1976**, *15*, 5631-5640.

[22] Gruning, N.M.; Du, D.; Keller, M.A.; Luisi, B.F.; Ralser, M. Inhibition of triosephosphate isomerase by phosphoenolpyruvate in the feedback-regulation of glycolysis. *Open Biolo.,* **2014**, *4*, 130232.

[23] Albery, W.J.; Knowles, J.R. Free-energy profile for the reaction catalyzed by triosephosphate isomerase. *Biochemistry,* **1976**, *15*, 5627-5631.

[24] Knowles, J.R.; Albery, W.J. Perfection in enzyme catalysis: the energetics of triosephosphate isomerase. *Acc. Chem. Res.,* **1977**, *10*, 105-111.

[25] Belasco, J.G.; Knowles, J.R. Direct observation of substrate distortion by triosephosphate isomerase using fourier transform infrared spectroscopy. *Biochemistry,* **1980**, *19*, 472-477.

[26] Lodi, P.J.; Chang, L.C.; Knowles, J.R.; Komives, E.A. Triosephosphate isomerase requires a positively charged active site: The role of lysine-12. *Biochemistry,* **1994**, *33*, 2809-2814.

[27] Kursula, I.; Partanen, S.; Lambeir, A.M.; Antonov, D.M.; Augustyns, K.; Wierenga, R. K. Structural determinants for ligand binding and catalysis of triosephosphate isomerase. *European J. Biochem.*, *FEBS,* **2001**, *268*, 5189-96.

[28] Krasnov, G.S.; Dmitriev, A.A.; Snezhkina, A.V.; Kudryavtseva, A.V. Deregulation of glycolysis in cancer: Glyceraldehyde-3-phosphate dehydrogenase as a therapeutic target. *Expert Opin. Ther. Targets,* **2013**, *17*, 681-93.